CFD Analysis of Oil Distribution in Oil-injected Screw Compressor

Jin-Wei ZHANG, Sheng-Hung HSIEH*, Chi-Shun HUANG

Hanbell Precise Machinery Co. Ltd.
Taoyuan City, Taiwan (R.O.C.)
Phone：+886-4-23501886#23355
Fax：+886-4-23501885
*E-mail：shhsieh@hanbell.com

ABSTRACT

Oil-injected screw compressor has been used in various industries. After decades of continuous research efforts by research teams around the world, the computer tools for rotor profile design, thermodynamic analysis, CFD/CAE calculation, and moving grid generation have been well developed and widely employed in design works. With assistance from the computer tools in performance simulation, designers could clearly understand internal phenomena of a screw compressor, as a reference for performance optimization design, and systematically carry out research works. One important issue inside an oil-injected screw compressor is about oil distribution. Different oil-injected positions and quantities cause different oil distribution inside the compressor. Therefore, the effects of oil sealing and lubrication change. Designers must understand how oil distribution is to deal with oil issues. In this study, CFD analysis was done with dynamic grid technology. Basic performance of screw compressor was calculated and compared with experiment data. Besides, three CFD models with different oil-injected paths were designed and analyzed. The influence of varying oil-injected conditions on oil distribution near contact line, sealing lines, blow holes, and end sides of inlet and outlet are shown in this study. They are used to explain how volumetric efficiency is affected. Especially for oil distribution near contact line, it not only affects volumetric efficiency, but also acts on the lubrication as rotor meshing.

1. INTRODUCTION

The operation of oil-injected screw compressor is based on deformable compression chambers constructed by the lobes or rotors and the case. The gas goes into compression chambers through the inlet port of case, and is compressed by the meshing rotors. During the compression process, oil is injected on a specific location. Oil lubricates the rotating rotors and decreases the temperature of the compressed gas to a safe working range. Finally, the compressed gas goes out of compression chambers through the outlet port of case. The flow path is shown in Figure 1. Study on oil-injected screw compressor usually considered the effects of oil-injection, and is carried out by thermodynamic analysis or CAE/CFD analysis. The goal is to get the performance of compressor, such as volumetric and isentropic efficiencies, and the forces or torque on rotors.

Based on thermodynamic analysis, Stosic *et al.*, (1992) performed a parametric study to investigate the oil-injection parameters on performance of compressor. Fujiwara *et al.*, (1995) obtained the correlations of the heat transfer coefficients between the compressed gas and oil inside an oil-injected screw compressor. Fleming *et al.*, (1995; 1998a; 1998b) studied the leakage paths inside the screw compressor and noted that the clearances of the leakage paths affect the performance of the screw compressor. Wu *et al.*, (2004; 2007) considered the relative motion between the compressed air and oil and calculated the mass flow rates at the leakage paths and at the outlet. Seshaiah *et al.*, (2007; 2010) calculated the mass flow rates of the compressed gas and the oil through the clearances of the leakage paths. They studied not only the effects of the clearance of the leakage paths on the performance of the compressor, but also the effects of the mass ratio of the compressed gas to oil on the temperature-time histories of the compressed air and oil. Based on CAE/CFD analysis, Kovacevic *et al.*, (2005; 2006; 2007; 2011) and Rane and Kovacevic (2017) developed and refined a procedure to generate dynamic meshes. The deformable meshes were shown to improve the accuracy of the calculations for the multiphase flow field. In addition to the flow field, the temperature distribution in the rotors, the deformations of rotors and the stresses in the solid parts of the screw compressor were also calculated.

Based on mesh generation tool of TwinMesh and the simulation tool of ANSYS, performance of screw compressor is calculated in this study. Three CFD models with different oil-injected locations were designed and analyzed. The influence of different oil-injected conditions on oil distribution near contact line, sealing lines, blow holes, and outlet ends of rotors are shown in this study.

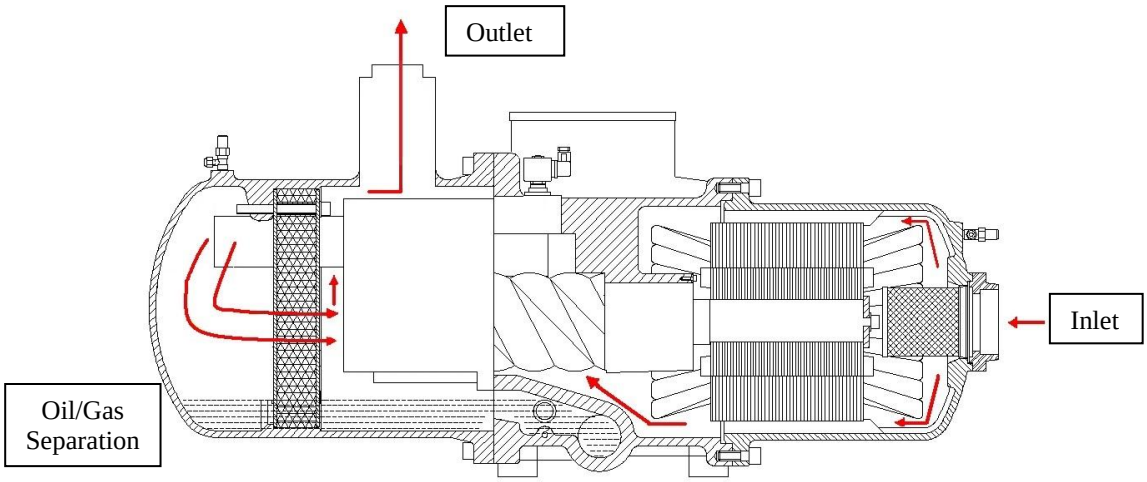

Figure 1: The schematic of an oil-injected screw compressor

2. THEORETICAL MODEL

An oil-injected screw compressor named RE-260 is analyzed in this study. Figure 2 (a) shows the main structures of compressor, including a pair of rotors, case, and outlet parts. A pair of "5x6" rotors and case construct the compression chambers. The gas goes through the inlet part of case and enters the compression chambers. After the gas pressure is increased enough, the compressed gas starts to flow to the next stage through the outlet part. In order to reduce the calculation time, the reduced 3D model is adapted and shown in Figure 2 (b). The 3D model is analyzed by ANSYS CFX. The conservation equations of continuity, momentum, and energy are solved. The turbulent flow and non-slip wall conditions are considered. The Multiphase module of ANSYS CFX is used to analyze the effect of oil-injection. The Volume of Fraction (VOF) is calculated and is used to explain the oil distribution.

(a) (b)

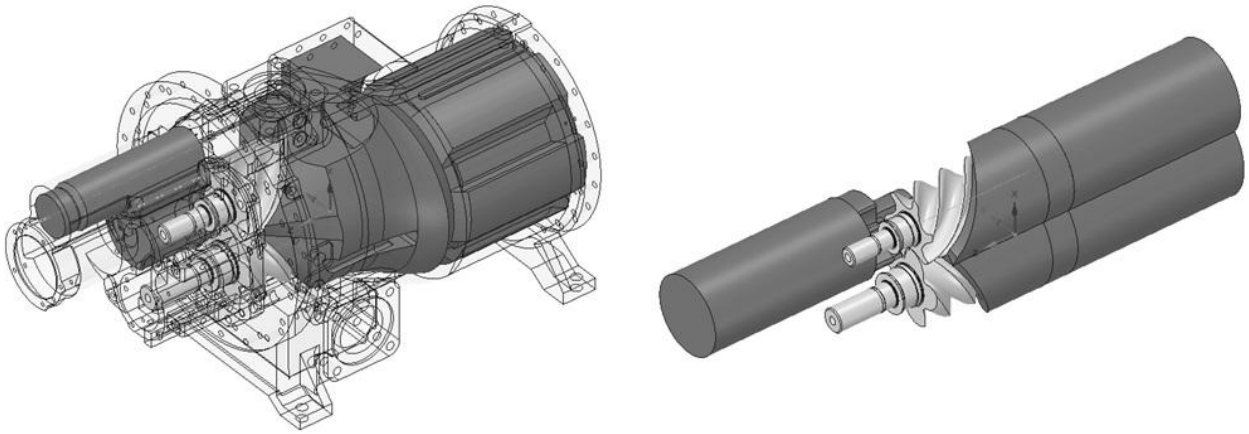

Figure 2: (a) Full and (b) reduced 3-D model of oil-injected screw compressor

The flow path is cut into dynamic and static mesh regions, as shown in Figure 3. Figure 3 (a) shows the dynamic mesh region, where is the compression chamber. The dynamic mesh is generated by TwinMesh. At first, 2D face

mesh of ends of rotors is obtained. Then, the whole 3D dynamic meshes are generated by the concept of sweep. With the dynamic mesh, the fluid phenomena inside compression chambers can be calculated by ANSYS CFX efficiently. Figure 3 (b) shows the static mesh regions, including the case and outlet part. The element number of the theoretical model is about 300,000 in static mesh region, and 2,000,000 in dynamic mesh region.

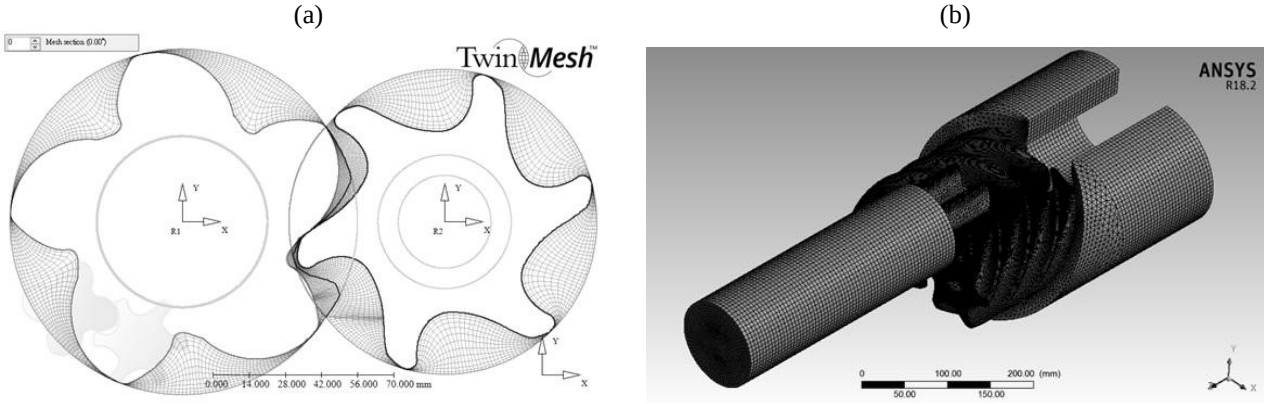

Figure 3: (a) Dynamic mesh and (b) static mesh of flow paths

In this study, theoretical models with three different oil-injected locations are designed. Figure 4 (a) shows the oil-injected location (a). The compression chamber just achieves the maximum volume. The oil is injected into the chamber on the male rotor side. At this moment, the rotation angle of male rotor is at (n) Degree. Figure 4 (b) shows the oil-injected location (b). The oil is injected into the chamber on the male rotor side. The rotation angle of male rotor is at (n + 72) Degree. Figure 4 (c) shows the oil-injected location (c). The oil is injected into the chamber on both male and female rotor sides. The rotation angle of male rotor is at (n + 144) Degree. Besides the different oil-injected locations, the different oil-injected flow-rates of 5, 15, and 25L/min are also considered on oil-injected location (b). Above mentioned oil-injected conditions are listed in Table 1. The calculation conditions of all models are 3,600rpm for rotational speed, 3.6bar for inlet pressure, and 9.8bar for outlet pressure.

Table 1: Oil injection conditions of theoretical models

Location shown in Figure. 4	Oil-injected flow-rate		
	5 L/min	15 L/min	25 L/min
(a)	--	◯	--
(b)	◯	◯	◯
(c)	--	◯	--

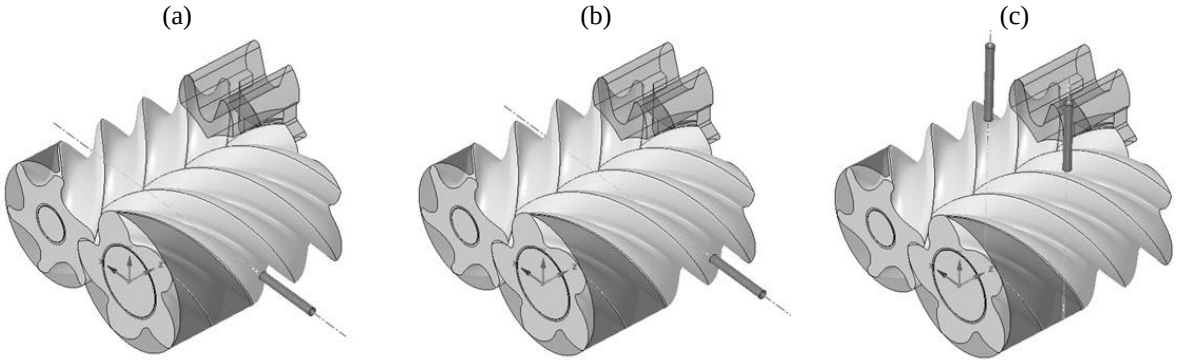

Figure 4: (a) Oil is injected on male rotor side. Male rotor is at (n^o) rotation angle. (b) Oil is injected on male rotor side. Male rotor is at ($n^o + 72^o$) rotation angle. (c) Oil is injected on both male and female rotor sides. Male rotor is at ($n^o + 144^o$) rotation angle.

3. RESULT AND DISCUSSION

The theoretical models listed in Table 1 are all calculated. The volumetric efficiencies are list in Table 2. As oil is injected on the location (b), the volumetric efficiencies are 90.5%, 91.2%, and 92.7% corresponding to oil-injected flow-rates of 5, 15, and 25L/min. Under the condition of oil-injected flow-rate of 15L/min, the volumetric efficiencies are 90.8%, 91.2% and 87.5% corresponding to the oil-injected location (a), (b) and (c). Volumetric efficiencies are affected by oil-injected location and flow-rate. Between the oil-injected flow-rates of 5 and 25L/min on location (b), the difference of volumetric efficiency is about 2.43%.

The values of total average gas torque are also list in Table 2. As oil is injected on the location (b), the values of total average gas torque are 103.7, 104.5, and 105.2N-m corresponding to oil-injected flow-rates of 5, 15, and 25L/min. Under the condition of oil-injected flow-rate of 15L/min, the values of total average gas torque are 105.1, 104.5, and 104.7N-m corresponding to the oil-injected location (a), (b) and (c). The values of total average gas torque are affected by oil-injected location and flow-rate. Between the oil-injected flow-rates of 5 and 25L/min on location (b), the difference of total average gas torque is about 1.43%.

Figure 5 shows the pressure curves of theoretical models with oil-injected flow-rates of 5 and 25L/min on location (b). The pressure curves are cut into inlet stage (A), compression stage (B), and outlet stage (C). The trends of the pressure curves in the inlet stage are quite the same. In the compression stage, the separation between two pressure curves appears after oil is injected. In the outlet stage, the separation between both pressure curves is clear. The pressure pulse appears for the structure effect. The amplitude of the pressure pulse would be influenced by oil, and is larger as more oil being injected.

Table 2: Volumetric efficiencies and total average gas torque

Performance	Location shown in Figure. 4	Oil-injected flow-rate		
		5 L/min	15 L/min	25 L/min
Volumetric Efficiency [%]	(a)	--	90.8	--
	(b)	90.5	91.2	92.7
	(c)	--	87.5	--
Total average gas torque [N-m]	(a)	--	105.1	--
	(b)	103.7	104.5	105.2
	(c)	--	104.7	--

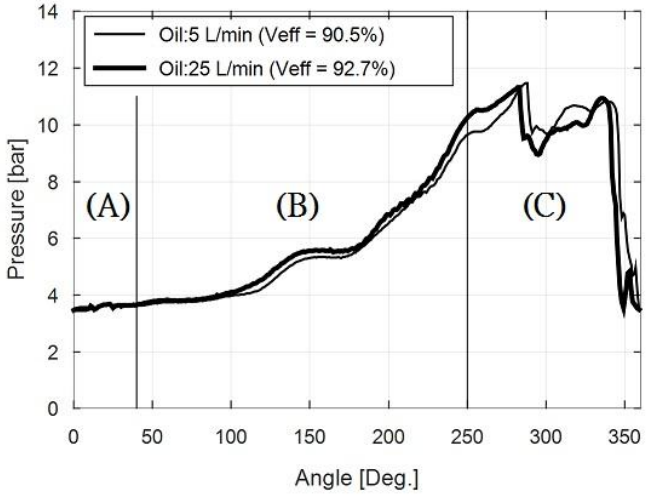

Figure 5: Pressure curves under oil-injected flow-rates of 5 and 25L/min

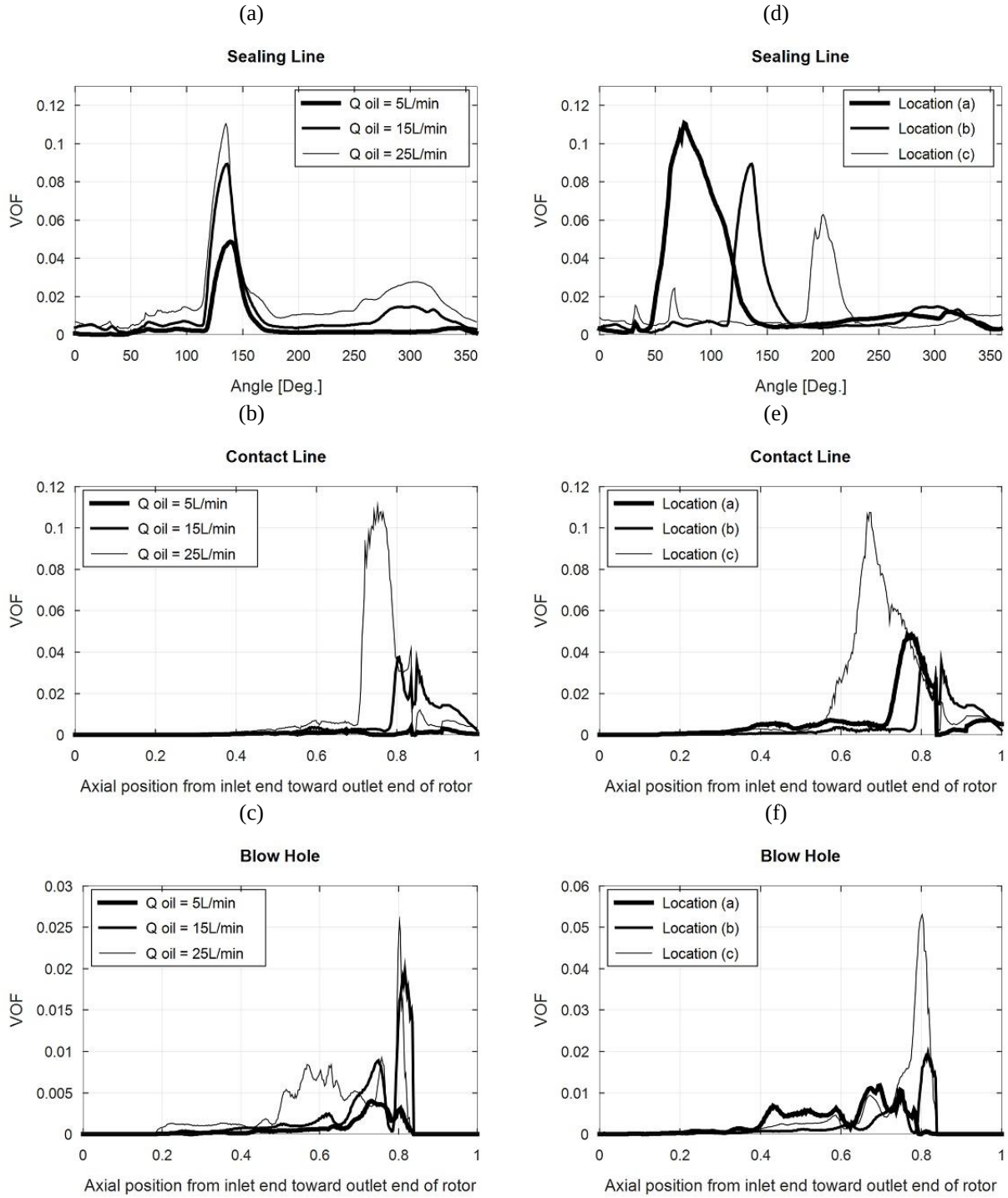

Figure 6: (a), (b), and (c) show volume of fraction of oil with different oil-injected flow-rates on location b. (d), (e), and (f) show volume of fraction of oil with oil-injected flow-rate of 15L/min on different locations.

The volume of fractions (VOFs) of oil on sealing line, contact line, and blow hole are shown in Figure 6. Figure 6 (a) and (d) show VOF curves of oil on sealing line. The x-axis denotes the rotation angle of male rotor. The y-axis denotes the average VOF of oil on sealing line corresponding to the rotation angle. When the lobe of rotor crosses the oil-injected location, the VOF of oil significantly increases. When the lobe moves forward, the injected oil spreads in the compression chamber, and the VOF of oil on sealing line decreases. In the outlet process, the oil starts to accumulate on sealing line. The increased VOF of oil is observable. Figure 6 (a) shows the VOF curves of oil on

sealing line with different oil-injected flow-rates on location (b). When the oil-injected flow-rate is larger, the VOF of oil on sealing is higher. Figure 6 (b) shows the VOF curves of oil on sealing line with oil-injected flow-rate of 15L/min on different locations. The position of maximum value on sealing line changes with the oil-injected location.

Figure 6 (b), (c), (e) and (f) show the VOF curves of oil on contact line and blow hole versus axial position from inlet end toward outlet end of rotor. In the range between inlet end and middle of rotor, this part of rotor experiences the inlet process and beginning of compression process. The oil just begins to be injected into compression chamber. The pressure differences between the chambers separated by contact line and blow hole are small. Therefore, less oil mixed with gas flows through contact line and blow hole. The VOFs of oil in this range are small. In the range between middle and outlet end of rotor, this part of rotor experiences the compression and outlet processes. The oil has already injected into compression chamber. The pressure differences between the chambers separated by contact line and blow hole are increased. More oil mixed with gas flows through contact line and blow hole. The VOF curves of oil begin to increase from the middle of rotor. The largest VOFs on contact line and blow hole appear when the part of rotor experiences outlet process. Figure 6 (b) and (c) show the VOF curves of oil on contact line and blow hole with different oil-injected flow-rates on location (b). In the range with significant values, the maximum value increases and the range becomes wider under larger oil-injected flow rate. Figure 6 (e) and (f) show the VOF curves of oil on contact line and blow hole with oil-injected flow-rate of 15L/min on different locations. In the range with significant values, the maximum value and the range are different between different oil-injected locations. The largest maximum value and widest range appear when oil is injected on location (c).

For the oil distribution on outlet ends of rotors, figure 7 (a) shows that most oil, which is injected from the side of male rotor, is located in the lobes which experience the last half of compression and outlet processes. The VOF is small in the lobes which experience inlet and the beginning of compression processes. These show that when oil is injected into the compression chamber, oil is not only thrown in radial direction, but also pushed toward the outlet end of rotor. Finally, the oil would be released through outlet port, as shown in Figure 7 (b).

(a) (b)

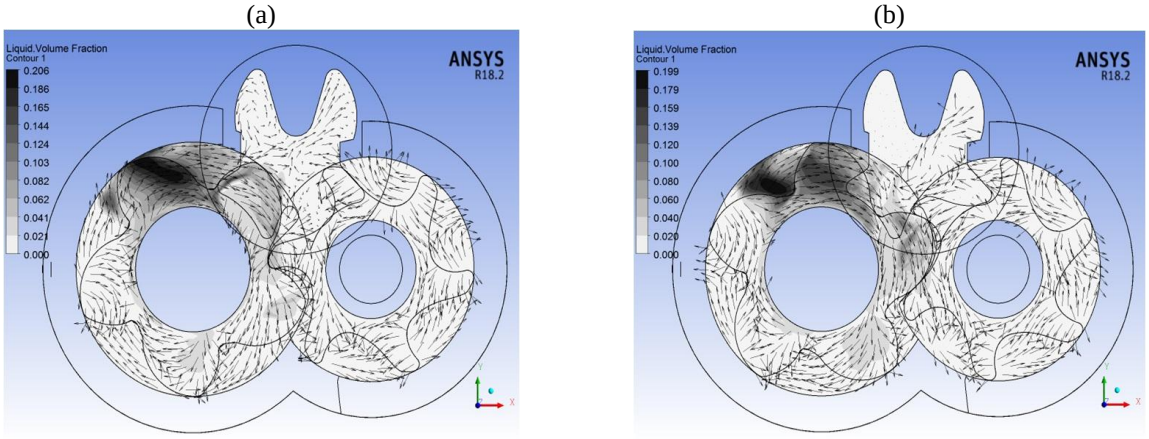

Figure 7: Volume of fraction of oil on the ends of rotors

The pressure information inside compression chamber is applied to calculate the forces acting on rotors. The radial and axial forces are listed in Table 3. In the model with oil-injected flow-rate of 5L/min on location (b), the radial force is 5.53±0.33kN and axial force is -2.24±0.21kN on male rotor. The radial force is 6.17±0.44kN and axial force is -0.51±0.05kN on female rotor. The radial force on female rotor is about 0.64kN larger than the one on male rotor. The axial force on male rotor is about 1.73kN larger than the one on female rotor. In the model with oil-injected flow-rate of 25L/min on location (b), the radial force is 5.60±0.34kN and axial force is -2.27±0.23kN on male rotor. The radial force is 6.26±0.51kN and axial force is -0.51±0.06kN on female rotor. The radial force on female rotor is about 0.66kN larger than the one on male rotor. The axial force on male rotor is about 1.76kN larger than the one on female rotor.

The pressure information could also be applied to calculate the gas torque acting on rotors. The average gas torque is listed in Table 3. The gas torque curves are shown in Figure 8. In the model with oil-injected flow-rate of 5L/min on

location (b), the total average gas torque is 103.71±9.54N-m. In the model with oil-injected flow-rate of 25L/min on location (b), the total average gas torque is 105.19±10.47N-m. The difference is about 1.43% between these two oil-injected flow-rates. Figure 8 (a) and (b) show that the trends of torque curves between these two oil-injected flow-rates are quite the same. The torque on male rotor is always larger than 0N-m. The one on female rotor is always smaller than 0N-m. These show that male and female rotors could rotate stably.

Table 3: Force and gas torque acting on rotors

		Oil Injection	5 Liter/min	25 Liter/min
Force [kN]	Male Rotor	radial direction	5.53±0.33	5.60±0.34
		axial direction	-2.24±0.21	-2.27±0.23
	Female Rotor	radial direction	6.17±0.44	6.26±0.51
		axial direction	-0.51±0.05	-0.51±0.06
Torque [N-m]	Male Rotor		84.58±7.76	86.03±8.61
	Female Rotor		-22.96±2.22	-22.99±2.60
	Total		103.71±9.54	105.19±10.47

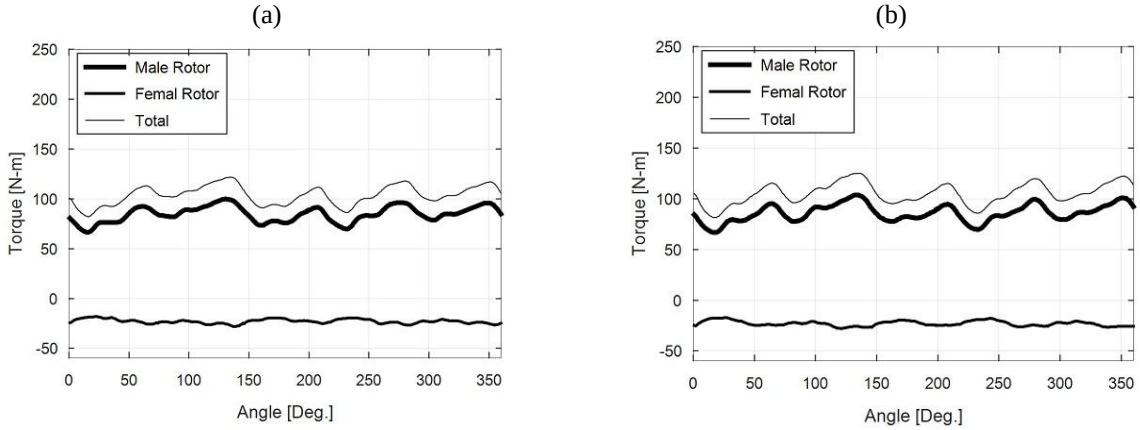

Figure 8: Gas torque curves under oil-injected flow-rates of (a) 5L/min and (b) 25L/min

4. CONCLUSIONS

The pressure curves, force on rotor, gas torque on rotor, and oil distribution inside oil-injected screw compressor are discovered. With the help of dynamic mesh and CFD tools, the models with different oil-injected flow-rates and locations are calculated. The performance of oil-injected screw compressor would be affected by different oil-injected flow-rates and locations. When oil-injected flow-rate changes from 5 to 25L/min, volumetric efficiency is about 2.43% increased and total gas torque is about 1.43% increased. Under oil-injected flow-rates of 5 and 25L/min on location (b), the trends of the pressure curves are quite the same in the inlet stage. In the compression stage, the separation between two pressure curves appears after oil is injected. In the outlet stage, the separation between both pressure curves is clear. The pressure pulse appears for the effect of structure. The amplitude of the pressure pulse would be influenced by oil, and is larger as more oil being injected.

When lobe of rotor crosses the oil-injected location, the value of VOF of oil on sealing line significantly increases. When the lobe moves forward, the injected oil spreads in the compression chamber, and the value of VOF of oil on sealing line decreases. In the outlet process, the oil starts to accumulate on sealing line. The increased value of VOF is observable. When the oil-injected flow-rate is larger, the value of VOF of oil on sealing is higher. The position of maximum value of VOF of oil on sealing line changes with the oil-injected location. In the range with significant values of VOF of oil on contact line and blow hole, the maximum value increases and the range becomes wider under larger oil-injected flow rate. The maximum value and the range are different between different oil-injected locations. The largest maximum value and widest range appear when oil is injected on designed location (c).

For the oil distribution on outlet ends of rotors, most oil is located in the lobes which experience the last half of compression and outlet processes. The VOF is small in the lobes which experience inlet and beginning of compression processes. When oil is injected into the compression chamber, oil is not only thrown in radial direction, but also pushed toward the outlet end of rotor. Finally, the oil would be released through outlet port.

REFERENCES

Fleming, J. S., & Tang, Y. (1995). The Analysis of Leakage in a Twin-Screw Compressor and Its Application to Performance Improvement. *Proceedings of the Institution of Mechanical Engineers Part E-Journal of Process Mechanical Engineering, 209*(E2), 125-136.

Fleming, J. S., Tang, Y., & Cook, G. (1998a). The twin helical screw compressor Part 1: development, applications and competitive position. *Proceedings of the Institution of Mechanical Engineers Part C-Journal of Mechanical Engineering Science, 212*(5), 355-367. doi:Doi 10.1243/0954406981521286

Fleming, J. S., Tang, Y., & Cook, G. (1998b). The twin helical screw compressor Part 2: a mathematical model of the working process. *Proceedings of the Institution of Mechanical Engineers Part C-Journal of Mechanical Engineering Science, 212*(5), 369-380. doi:Doi 10.1243/0954406981521295

Fujiwara, M., & Osada, Y. (1995). Performance Analysis of an Oil-Injected Screw Compressor and Its Application. *International Journal of Refrigeration-Revue Internationale Du Froid, 18*(4), 220-227.

Kovacevic, A. (2005). Boundary adaptation in grid generation for CFD analysis of screw compressors. *International Journal for Numerical Methods in Engineering, 64*(3), 401-426. doi:Doi 10.1002/Nme.1376

Kovacevic, A., Stosic, N., Mujic, E., & Smith, I. K. (2007). Cfd Integrated Design of Screw Compressors. *Engineering Applications of Computational Fluid Mechanics, 1*(2), 96-108.

Kovacevic, A., Stosic, N., Mujic, E., Smith, I. K., & Guerrato, D. (2011). Extending the role of computational fluid dynamics in screw machines. *Proceedings of the Institution of Mechanical Engineers Part E-Journal of Process Mechanical Engineering, 225*(E2), 83-97. doi:Doi 10.1177/0954408910397586

Kovacevic, A., Stosic, N., & Smith, I. K. (2006). Numerical simulation of combined screw compressor-expander machines for use in high pressure refrigeration systems. *Simulation Modelling Practice and Theory, 14*(8), 1143-1154. doi:DOI 10.1016/j.simpat.2006.09.004

Rane, S., Kovacevic, A. (2017). Application of numerical grid generation for improved CFD analysis of multiphase screw machines. *Materials Science and Engineering:10th International Conference on Compressors and their Systems*. doi:10.1088/1757-899X/232/1/012017

Seshaiah, N., Ghosh, S. K., Sahoo, R. K., & Sarangi, S. K. (2007). Mathematical modeling of the working cycle of oil injected rotary twin screw compressor. *Applied Thermal Engineering, 27*(1), 145-155. doi:DOI 10.1016/j.applthermaleng.2006.05.007

Seshaiah, N., Sahoo, R. K., & Sarangi, S. K. (2010). Theoretical and experimental studies on oil injected twin-screw air compressor when compressing different light and heavy gases. *Applied Thermal Engineering, 30*(4), 327-339. doi:DOI 10.1016/j.applthermaleng.2009.09.010

Stosic, N., Milutinovic, L., Hanjalic, K., & Kovacevic, A. (1992). Investigation of the Influence of Oil Injection Upon the Screw Compressor Working Process. *International Journal of Refrigeration-Revue Internationale Du Froid, 15*(4), 206-220.

Wu, H., Li, H. F., & Xing, Z. W. (2007). Theoretical and experimental research on the working process of screw refrigeration compressor under superfeed condition. *International Journal of Refrigeration-Revue Internationale Du Froid, 30*(8), 1329-1335. doi:DOI 10.1016/j.ijrefrig.2007.04.005

Wu, H. G., Xing, Z. W., & Shu, P. C. (2004). Theoretical and experimental study on indicator diagram of twin screw refrigeration compressor. *International Journal of Refrigeration-Revue Internationale Du Froid, 27*(4), 331-338. doi:DOI 10.1016/j.ijrefrig.2004.01.004